doi:10.1016/j.jmb.2005.12.033 J. Mol. Biol. (2006) 357, 115–126

JMB

Available online at www.sciencedirect.com

SCIENCE DIRECT®

ELSEVIER

Model for RNA Binding and the Catalytic Site of the RNase Kid of the Bacterial *parD* Toxin–Antitoxin System

Monique B. Kamphuis[1], Alexandre M. J. J. Bonvin[1], Maria Chiara Monti[3] Marc Lemonnier[2], Ana Muñoz-Gómez[2], Robert H. H. van den Heuvel[3] Ramón Díaz-Orejas[2] and Rolf Boelens[1]*

[1]*Bijvoet Center for Biomolecular Research, Department of NMR Spectroscopy, Utrecht University, Padualaan 8, 3584 CH Utrecht, The Netherlands*

[2]*Centro de Investigaciones Biológicas, Departamento de Microbiología Molecular Ramiro de Maeztu 9, 28040 Madrid, Spain*

[3]*Bijvoet Center for Biomolecular Research, Department of Biomolecular Mass Spectrometry, Utrecht University, Sorbonnelaan 16 3584 CA Utrecht, The Netherlands*

**Corresponding author*

The toxin Kid and antitoxin Kis are encoded by the *parD* operon of *Escherichia coli* plasmid R1. Kid and its chromosomal homologues MazF and ChpBK have been shown to inhibit protein synthesis in cell extracts and to act as ribosome-independent endoribonucleases *in vitro*. Kid cleaves RNA preferentially at the 5′ side of the A residue in the nucleotide sequence 5′-UA(A/C)-3′ of single-stranded regions. Here, we show that RNA cleavage by Kid yields two fragments with a 2′:3′-cyclic phosphate group and a free 5′-OH group, respectively. The cleavage mechanism is similar to that of RNases A and T1, involving the uracil 2′-OH group. *Via* NMR titration studies with an uncleavable RNA mimic, we demonstrate that residues of both monomers of the Kid dimer together form a concatenated RNA-binding surface. Docking calculations based on the NMR chemical shifts, the cleavage mechanism and previously reported mutagenesis data provide a detailed picture of the position of the AUACA fragment within the binding pocket. We propose that residues D75, R73 and H17 form the active site of the Kid toxin, where D75 and R73 are the catalytic base and acid, respectively. The RNA sequence specificity is defined by residues T46, S47, A55, F57, T69, V71 and R73. Our data show the importance of these residues for Kid function, and the implications of our results for related toxins, such as MazF, CcdB and RelE, are discussed.

Keywords: docking; NMR; protein–RNA complex; ribonuclease; toxin–antitoxin

Introduction

Toxin–antitoxin (TA) systems are involved in cell growth arrest and possible cell death.[1,2] These systems, discovered originally in plasmids, are conserved in bacterial as well as archaeal genomes.[2,3] In general, TA systems consist of two genes that encode a stable toxin and an unstable antitoxin.[2,4] The antitoxin neutralises the toxicity by forming a protein complex with the toxin, but is degraded by cellular proteases and has to be replenished constantly.[2] This explains how TA loci on plasmids increase plasmid maintenance by preventing the growth of plasmid-free progeny. Chromosomal TA systems might provide a control mechanism for free-living prokaryotes to cope with nutritional stress.[2,5] Interestingly, several bacterial TA systems have been reported to function in yeast and induce apoptosis in human cells.[6–8] These results suggest that bacterial TA systems trigger a universal mechanism that can result in cell death in prokaryotes and in eukaryotes.

A well-characterised TA system is the *Escherichia coli* Kid–Kis system. The toxin Kid (PemK) and antitoxin Kis (PemI) are encoded by the *parD* operon of plasmid R1,[9] which is identical with *pem* on plasmid R100.[10] Kid inhibits cell growth in *E. coli* and Kis counteracts this effect.[11] The coordinate action of Kid and Kis has been shown to autoregulate *parD* at the level of transcription.[12] The crystal structure of the Kid protein has been determined, revealing a symmetric dimer.[13,14] Also, the structure of a complex of MazF (ChpAK)

Abbreviations used: AIR, ambiguous interaction restraint; HSQC, heteronuclear single quantum coherence; Kid, killing determinant; Kis, killing suppressor; TA, toxin–antitoxin.

E-mail address of the corresponding author: r.boelens@chem.uu.nl

and MazE (ChpAI), chromosomal homologues of Kid and Kis, has been described.[15]

MazF and ChpBK, another chromosomal homologue of Kid, have been demonstrated to cleave translated mRNAs and block protein synthesis, a blockage that is counteracted by tmRNA.[16] In cell extracts, Kid, MazF and ChpBK have been shown to be able to inhibit protein synthesis and these proteins can act both *in vitro* and *in vivo* as endoribonucleases able to cleave RNA in the absence of ribosomes.[17–23] The Kid toxin cleaves RNA preferentially at the 5′ side of the A residue in the nucleotide sequence 5′-UA(A/C)-3′ of single-stranded regions, although cleavage in double-stranded regions,[17] and at the 3′ side of the adenosine base, has been observed as well.[17,20] The presence of the antitoxins Kis and MazE prevents RNA cleavage by Kid and MazF, respectively.[17,18,20,21,23]

The mechanism of RNA binding and cleavage by the Kid toxin is not known. In this work, we use 1D ^{1}H-NMR spectroscopy and electrospray ionisation mass spectrometry to demonstrate that Kid cleaves the dinucleotide UpA and the 5 nt RNA fragment AUACA, yielding two products with a uracil 2′:3′-cyclic phosphate group at one side and an adenosine base with a free 5′-OH group at the other side. We show that the uracil 2′-OH group is absolutely essential for cleavage, and investigate the inhibitory effect of the antitoxin Kis. Using NMR spectroscopy, we identify the residues of Kid involved in interaction with the RNA-dU and DNA fragments AdUACA and d(AUACA) and determine the nucleotide-binding site of the Kid protein. These data are converted into a model of the Kid–RNA complex using the program HADDOCK, revealing that D75 and R73 are the catalytic residues of Kid responsible for its RNA cleavage activity, while H17 stabilises the complex, and that sequence-specific cleavage takes place due to interactions of Kid residues T46, S47, A55, F57, T69, V71 and R73 with the RNA nucleotides UA(A/C).

Results and Discussion

RNA cleavage by Kid yields a 2′:3′-cyclic phosphate group and a 5′-OH group, and involves the uracil 2′-OH

It has been shown recently that the Kid toxin cleaves RNA preferentially at the 5′ side of the A residue in the nucleotide sequence 5′-UA(A/C)-3′.[17,20] To characterise the mechanism of RNA cleavage by Kid, the cleavage of the 5 nt RNA (AUACA) and RNA-dU (AdUACA) fragments was investigated with ^{1}H-NMR spectroscopy and electrospray ionisation mass spectrometry. A series of 1D NMR spectra was recorded during AUACA cleavage and the decrease of substrate and build-up of products were followed (Figure 1(a)). Kid cleaves the RNA oligonucleotide with a catalytic efficiency (k_{cat}/K_m) of 0.78 $M^{-1}\,s^{-1}$ (K_m = 202 μM, k_{cat} = 0.00016 s^{-1}). Mass spectrometry revealed that the AUACA (molecular mass 1536.3 Da) cleavage takes place uniquely between uracil and adenosine, yielding two cleavage products with a molecular mass of 636.1 Da and 902.2 Da, corresponding to AU with a 2′:3′-cyclic phosphate group at the uracil and ACA with a free 5′-OH group on the first adenosine (Figure 1(c)). Monitoring the RNA sample without addition of protein showed no degradation during the time of the experiment. The natural inhibitor of the Kid toxin, the antitoxin Kis, has been shown to inhibit the RNA cleavage activity of Kid efficiently. We repeated the NMR and mass spectrometry cleavage experiments by supplying varying amounts of Kis to the RNA sample prior to the addition of the Kid protein. Indeed, RNA cleavage was suppressed strongly even in the presence of a molar ratio of Kis to Kid of only 0.3:1. To examine the role of the 2′-OH group of the uracil nucleotide in the RNA cleavage mechanism, the cleavage of the RNA-dU oligonucleotide (AdUACA, molecular mass 1520.3 Da) was followed. After incubation of RNA-dU with Kid for 30 min, no cleavage product was detected in the mass spectrum (Figure 1(d)), indicating the importance of the uracil 2′-OH group. The DNA (d(AUACA)) fragment was not cleaved by Kid either. The ability of Kid to cleave the minimal substrate UpA was demonstrated using ^{1}H-NMR spectroscopy. Figure 1(b) clearly shows that 2′:3′-cUMP is formed upon UpA cleavage and 5′-AMP is not. This fits with the mass spectrometry result obtained for AUACA cleavage. Thus, RNA cleavage by Kid results in a 2′:3′-cyclic phosphate group at one side and a free 5′-OH group at the other side, and the 2′-OH group of the uracil sugar ring is absolutely essential.

Cleavage by the well-studied RNase A and RNase T1 yields the same kind of products as determined for Kid, i.e. a 2′:3′-cyclic phosphate group and a 5′-OH group, and involves an essential 2′-hydroxyl group.[24] Apparently, Kid uses an enzymatic mechanism for the cleavage of phosphodiester linkages similar to RNase A and RNase T1. The RNase A and RNase T1 reactions involve a transphosphorylation step in which the 2′-OH group in RNA is deprotonated by a catalytic base to perform a nucleophilic attack on the electrophilic phosphorus. A catalytic acid donates a hydrogen atom to the 5′-leaving group. In the readily reversible second step, a 3′-monophosphate nucleotide is formed by hydrolysis of the 2′:3′-cyclophosphate group.[24–27] Similar results were published recently for the proteins MazF and ChpBK, chromosomal homologues of Kid.[21,22] The catalytic efficiency of 0.78 $M^{-1}\,s^{-1}$ determined for Kid is rather poor compared to the catalytic efficiency of 1×10^6 $M^{-1}\,s^{-1}$ of RNase T1 for GpU cleavage[27] or the catalytic efficiency of RNase A towards UpA (3.5×10^6 $M^{-1}\,s^{-1}$) and CpA (4.6×10^6 $M^{-1}\,s^{-1}$).[28] Recently, after the initial submission of our manuscript, Pimentel *et al.* studied the sequence specificity of the RNA cleavage reaction by Kid and

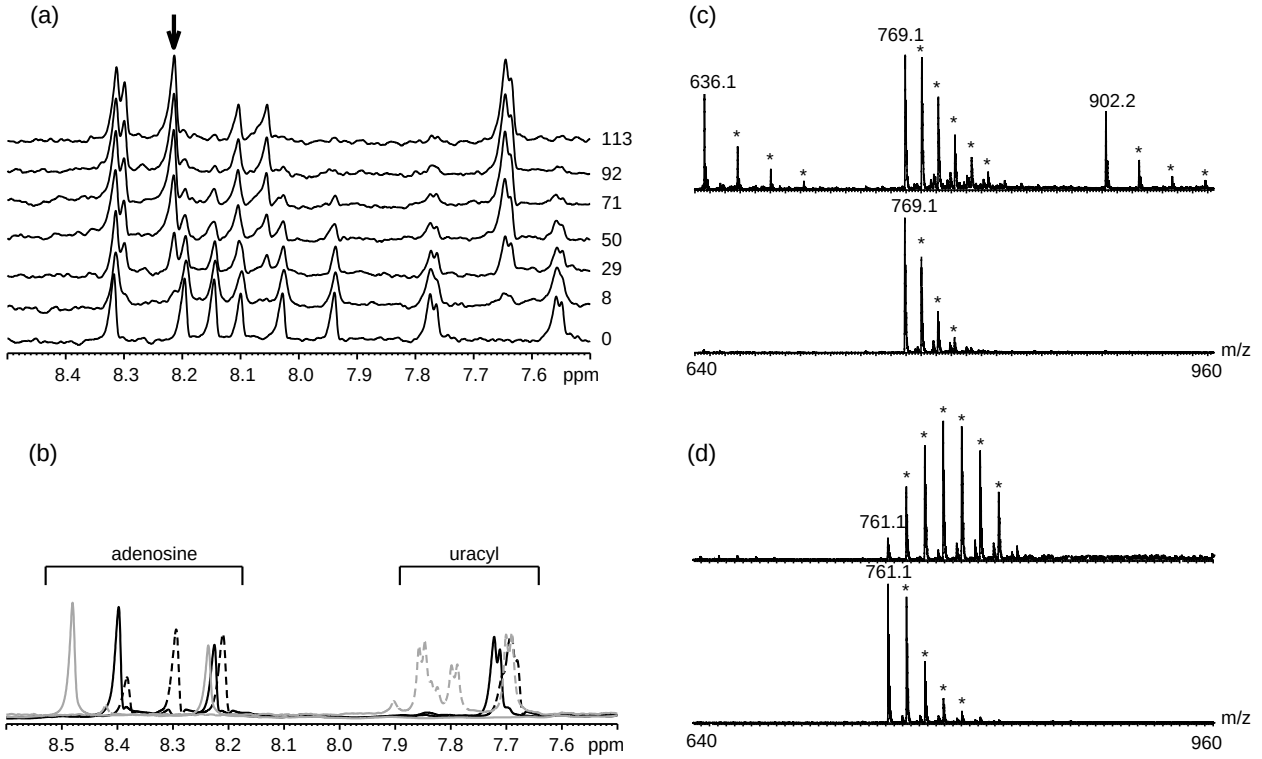

Figure 1. RNA cleavage by the toxin Kid. (a) AUACA cleavage followed in time by ^{1}H-NMR spectra of the aromatic protons of the RNA bases. The number on the right indicates the minutes elapsed after addition of the Kid protein. The arising peak at 8.21 ppm, indicated by an arrow, was used to calculate the catalytic efficiency of Kid. (b) Overlay of ^{1}H-NMR spectra of UpA (black, continuous), UpA cleavage products (black, broken), 5′-AMP (grey, continuous) and the mixture of 2′:3′-cUMP/3′-UMP/2′-UMP/U (grey, broken). The regions where adenosine and uracil proton peaks are located are indicated. The peaks of the mixture correspond to 3′-UMP at 7.85 ppm, uracil at 7.83 ppm, 2′-UMP at 7.79 ppm and 2′:3′-cUMP at 7.69 ppm. (c) Electrospray mass spectrometry spectra of AUACA incubated with Kid for 1 min. (lower panel) and 30 min (upper panel). The lower panel shows the doubly charged peaks of the intact RNA at m/z 769.1 and its sodium adducts (*). After 30 min of incubation (upper panel) the monocharged cleavage products were measured: The peak at m/z 636.1 was assigned to the fragment AU with a 2′:3′-cyclic phosphate and the peak at m/z 902.2 to ACA with a free 5′-OH. (d) Electrospray mass spectrometry spectra of AdUACA incubated with Kid for 1 min. (lower panel) and 30 min. (upper panel). Both panels show the doubly charged peaks of the intact RNA-dU at m/z 761.1 and its sodium adducts (*).

found that Kid recognises the 5′-UUACU-3′ sequence,[19] which contains the central UAC nucleotides as we used in our NMR study. A preliminary assay by mass spectrometry showed that the cleavage of the UUACU RNA fragment is 100 times more efficient than cleavage of AUACA. Possibly, a particular RNA conformation present in a native RNA sequence would further stimulate the catalytic efficiency.

RNA-binding site of the Kid dimer revealed: both monomers are involved

Direct observation of RNA binding to Kid *via* titrations followed by ^{1}H–^{15}N heteronuclear single quantum coherence (HSQC) spectra was not feasible, since the RNA oligonucleotide is cleaved by Kid. Therefore, RNA-dU (AdUACA) and DNA (d(AUACA)) oligonucleotides were used to map the nucleotide-binding site of the Kid toxin. The amount of oligonucleotide was increased up to a final molar ratio of ^{15}N-Kid:oligonucleotide of 1:2 for RNA-dU and 1:4 for DNA. Figure 2 presents the spectra of the RNA-dU experiment. The composite ^{15}N/^{1}H chemical shift perturbations are shown in Figure 3(a) and (b) for the RNA-dU and DNA titration, respectively. RNA-dU and DNA binding involve almost the same residues of Kid, coinciding with a positively charged patch on the Kid surface. The interaction of Kid with RNA-dU is much tighter than with DNA, as the amide atoms of Kid display intermediate exchange behaviour upon RNA-dU binding, while being almost all in fast exchange mode upon DNA binding. The 2′-OH groups of RNA-dU might account for this effect by enabling the formation of additional hydrogen bonds. A further increase can be expected for RNA substrates with the additional 2′-OH group at the catalytic uracil.

The results obtained with RNA-dU (Figure 3(a)) are mapped on the Kid structure in Figure 4(a) and (b). The close match of the secondary structures of Kid obtained by X-ray and NMR (data not shown) indicates a high level of structural similarity between the crystal and solution states of Kid. Therefore, the 3D crystal structure is used for the

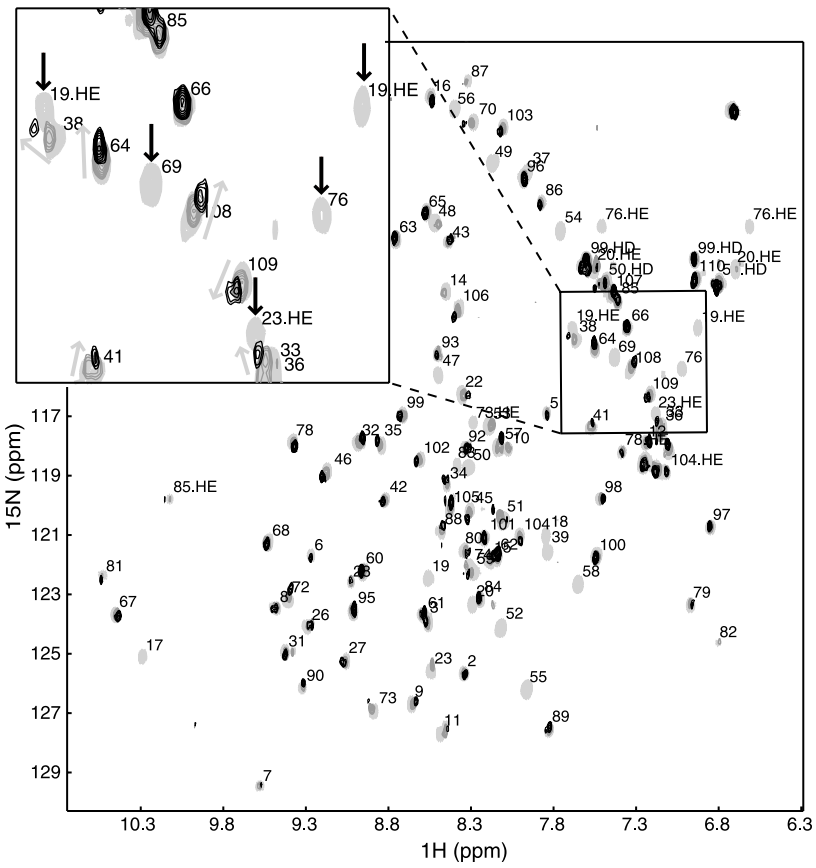

Figure 2. Overlay of ^{1}H–^{15}N HSQC spectra of the protein Kid, pure (light grey) and with RNA-dU added up to RNA-dU:Kid ratios of 0.5:1 (dark grey) and 2:1 (black). In the enlargement, NH peaks disappearing upon addition of RNA-dU are indicated by black arrows and the directions of the chemical shift perturbations of the shifting peaks are indicated by light grey arrows.

interpretation of our data concerning Kid in solution. The Kid residues involved in RNA-dU binding cluster into five sequence-based groups (Figure 4(b)). Cluster #1 is the loop containing residues S10, L11, T14, H17, E18, Q19 (backbone (bb) and side-chain (sc) amides), Q20 (bb and sc), T22 and R23 (bb and sc). Cluster #2 consists of five residues, V36, T37, R38 (bb and sc), L39 and V41, located at the end of the first α-helix. Cluster #3 is the loop comprising residues S47, G48, G49, N50 (bb and sc), F51, A52, R53 (bb), T54, A55, G56, A58 and V59.The turn/β-sheet/turn structure of cluster #4 is formed by residues T69, G70, V71, R73 (bb and sc), C74, D75 and Q76 (bb and sc), and the small α-helix formed by residues M82 and K83 (bb) is cluster #5.Clusters #1, #3 and #4 of monomer A cover a concatenated surface area together with clusters #2 and #5 of monomer B, forming the first RNA-binding site. The second RNA-binding site consists of clusters #2 and #5 of monomer A, and clusters #1, #3 and #4 of monomer B. This shows that both monomers are needed to form one RNA-binding site. This implies that Kid is toxic for bacteria cells only in its dimeric form, in contrast to RNase T1 and RNase A. Since the Kid dimer is symmetric, it contains two identical RNA-binding sites. To determine whether both of them can accommodate an RNA molecule at the same time, we used native mass spectrometry. Under pseudo-physiological conditions (250 mM ammonium acetate, pH 6.8), the mass spectra of Kid clearly showed the presence of both monomeric and dimeric protein. Upon the addition of a twofold molar excess of RNA, a complex was observed between the Kid dimer and a single RNA molecule (data not shown). Even at a tenfold molar excess of RNA, only the interaction with a single RNA molecule was observed. No complex between Kid monomer and RNA was detected. Thus, the two RNA-binding sites in the Kid dimer cannot be occupied simultaneously.

The five clusters involved in RNA-dU binding by Kid are not all similarly important for the activity of the toxin. Previously, a number of non-toxic Kid mutants has been obtained.[14,29] The residues identified in the mutagenesis study to be essential for the toxicity of the Kid protein almost all belong to clusters #1, #4 and #5 of the described RNA-binding pocket of Kid. Only the buried residue T29 does not show a chemical shift perturbation, and residue P94 could not be observed in the NMR spectra because it lacks an amide proton. Apparently, the precise amino acid composition of clusters #2 and #3 is not essential for Kid cleavage activity.

Comparison of the crystal structures of free Kid[14] and its chromosomal homologue MazF in complex with the antitoxin MazE[15] shows that the main difference between the structures is the "opening" of the loop comprising residues 10 to 21 (cluster #1) in both monomers. Because of the structural and functional resemblance of the toxins Kid and MazF, and the antitoxins Kis and MazE, respectively, it is likely that the antitoxin Kis binds to Kid in a similar

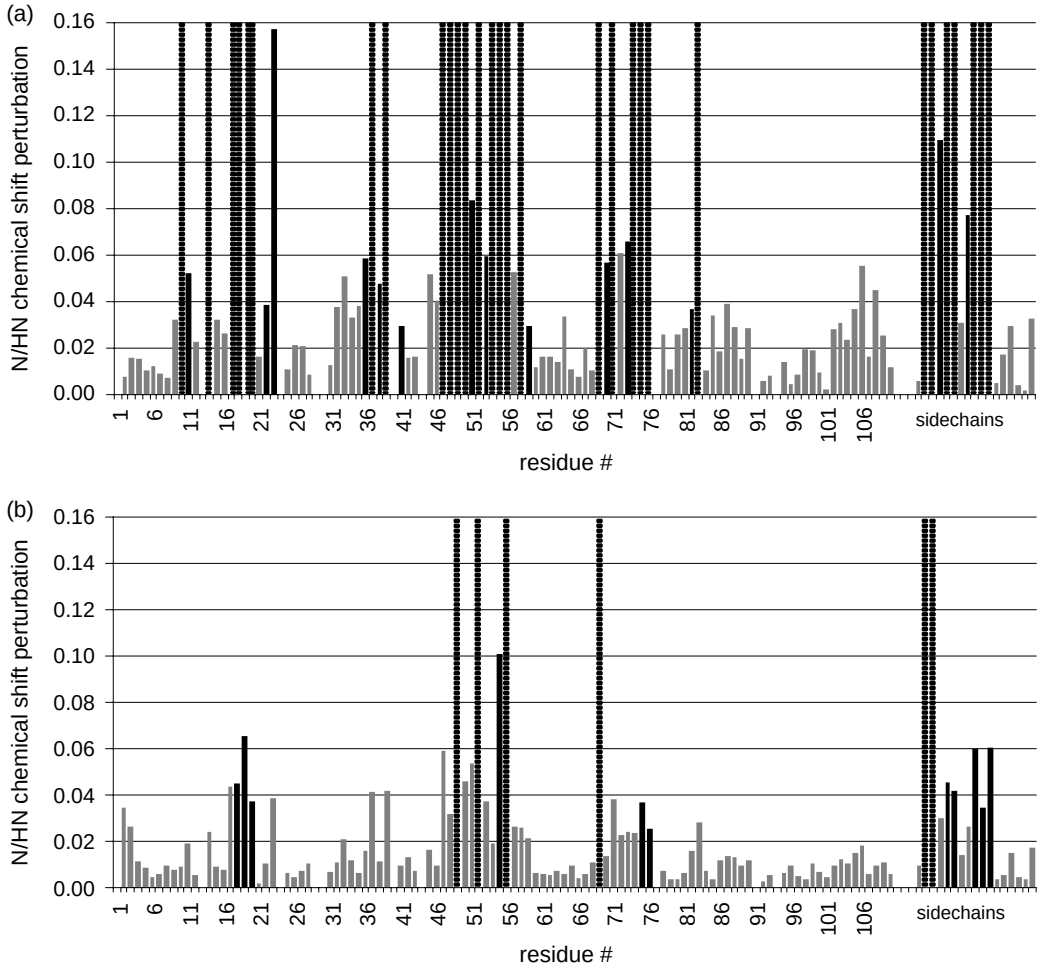

Figure 3. Kid residues involved in RNA-dU and DNA binding. (a) Chemical shift perturbation diagram of Kid residues upon addition of RNA-dU (RNA-dU/Kid ratio = 2:1). (b) Chemical shift perturbation diagram of Kid residues upon addition of DNA (DNA/Kid ratio = 4:1). The shifts of residues in fast exchange are shown in grey and those of residues in fast to intermediate exchange are shown in black. The broken lines indicate disappearing residues in intermediate exchange. Chemical shift changes of the side-chain NHs of W7, Q19 (2×), Q20 (2×), R23, R38, N50 (2×), R73, Q76 (2×), R78, R85, N99 (2×) and R104 are depicted as well. Residues 29 and 91 and the side-chains of residues R3, N34, R35, R53, R67, R89 and R92, which could not be assigned unambiguously, do not show chemical shift perturbations upon addition of RNA-dU or DNA. Proline residues are not observed (residues 13, 24, 30, 40, 44, 77 and 94).

way as MazE binds to MazF. The C-terminal tail of the antitoxin will partly occupy one of the revealed RNA-binding sites, while imposing the opening of both "cluster #1 loops", thereby disrupting the second RNA-binding pocket as well. Therefore, binding of only one Kis protein will be sufficient to inhibit the RNA cleavage activity of a Kid dimer efficiently. This fits well with the previously described result, that a molar ratio of Kis to Kid of only 0.3:1 strongly suppressed the RNA cleavage activity of Kid.

A model of the Kid–RNA complex

The revealed RNA-binding site was used to dock the model RNA oligonucleotide (AUACA) in the RNA-binding pocket of the Kid protein, using the program HADDOCK.[30] A total of 17 ambiguous interaction restraints (AIRs) were defined from the solvent-accessible Kid residues displaying intermediate exchange behaviour (Table 1) to the five RNA nucleotides. The loop containing residues S47 to A55 was defined to be passive instead of active, because ^{15}N-NMR relaxation experiments indicate that this loop is highly flexible (M.B.K., unpublished results). Residue A58, located in a β-strand beneath this loop, was defined passive as well (see Materials and Methods). Six AIRs were introduced from the bases of the three central nucleotides UAC of the RNA fragment to the selected Kid residues and their structural neighbours. Furthermore, the described enzymatic mechanism for the cleavage of 5′-UA-3′ linkages by Kid implies that a negatively charged residue as catalytic base deprotonates the 2′-OH group of uracil and that a positively charged residue as catalytic acid donates a proton to the leaving 5′-O of adenosine. The negatively charged residues determined to be essential for Kid toxicity

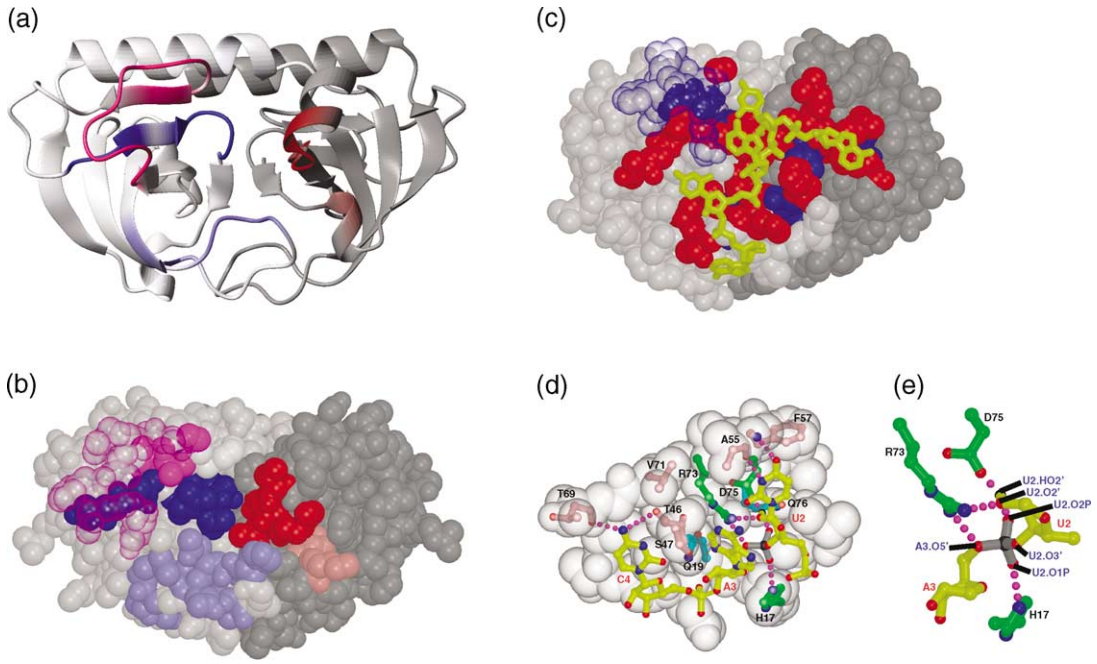

Figure 4. RNA-binding pocket and active site of Kid. Residues displaying intermediate exchange upon RNA-dU binding are mapped on a ribbon (a) and space-filling (b) representation of the crystal structure of the Kid dimer (PDB code 1M1F). The two monomers are coloured light grey and dark grey. The residues in intermediate exchange are clustered based on sequence: cluster #1 (residues 10–23) is shown in light blue, cluster #2 (residues 36–41) in red, cluster #3 (residues 47–59) in magenta, cluster #4 (residues 69–76) in dark blue and cluster #5 (residues 82–83) in pink. Clusters #1, #3 and #4 are located on monomer A and clusters #2 and #5 on monomer B. Since Kid exists as a symmetric dimer, two sets of residues can be distinguished that are both visible in (a). For clarity, however, only one of those sets is coloured. In (b), the loop in cluster 3 is transparent to show cluster 4 lying partly behind it. (c) Model of the Kid-RNA complex obtained with HADDOCK (PDB code 2C06). The RNA fragment is coloured yellow, the two Kid monomers are coloured light and dark grey, and the active Kid residues are coloured red (HADDOCK definition; see Table 1 and the text for details). The other Kid residues displaying intermediate exchange are shown in blue. The conformation of the loop containing residues 47-55 (transparent) has changed compared to (b). (d) Hydrogen bonds within the RNA-binding site of Kid involved in selective 5′-UA(A/C)-3′ recognition and UA cleavage, as obtained with HADDOCK. Part of the RNA-binding pocket is depicted in space-fill representation with the 5′-UAC-3′ fragment and important Kid residues in ball-and-stick. Nitrogen atoms are coloured blue and oxygen atoms are coloured red. The RNA fragment is shown in yellow with the phosphate group at the cleavage site in grey. T46/S47/A55/F57/T69/V71 (pink) play a role in selective recognition, while H17/R73/D75 (green) are involved in RNA cleavage (see the text for details). Q19 and Q76 are coloured cyan. Hydrogen bonds are shown as broken purple lines (see Table 2). (e) Detailed view of the catalytic site of Kid. Panel (a) was generated with the program MOLMOL (version 2K.1 by Reto Koradi) and (b), (c), (d) and (e) with MOLSCRIPT[52] and Raster3D.[53]

Table 1. Active and passive Kid residues used in HADDOCK[30]

A. *Active residues*
Monomer A: S10, T14, H17, Q19, Q20, T22, R23, T69, G70, V71, R73, D75, Q76
Monomer B: V36, T37, R38, K83
B. *Passive residues*
Monomer A: L8, D12, P13, A15, G16, G21, P24, V45, T46, S47, G48, G49, N50, F51, A52, R53, T54, A55, G56, F57, A58, S60, D62, I66, R67, T68, R85, E100, R104
Monomer B: W7, D12, P13, A32, F33, N34, R35, L39, D81, A84, R85, G86, G87

The active residues are solvent-accessible residues that display intermediate exchange behaviour during the NMR titration experiment. The passive residues are solvent-accessible residues that surround the active residues. See Materials and Methods for details.

in the previously reported mutagenesis study are E18, D75 and D81, whereas the positively charged residues are R73 and R85.[29] In that study, it was shown that E18K, R73H, D75N, D81N, R85W and R85Q mutations resulted in inactive Kid. On the basis of this information, two additional AIRs were defined (see Materials and Methods for details). The docking process driven by those 25 AIRs resulted in a lowest energy cluster containing 34 structures. After visual inspection, 30 structures were selected as input for a second docking run to obtain a proper geometry of the RNA within the active site of Kid. For this, three extra AIRs were added, since the Kid cleavage mechanism implies that during the pentavalent transition state, hydrogen bonds are present between uracil 2′-O and a positively charged proton of Kid, between adenosine O1P and a HN or HO-atom of Kid, and between uracil 2′-OH and adenosine O2P (in analogy to RNases A

Table 2. KID–RNA intermolecular contact statistics

Kid atom	RNA atom	Distance (Å)	#[a]
A. *Hydrogen bonds (proton–acceptor distance ≤2.7 Å)*			
D12.OD*	A5.HO2′	2.05±0.05	6
H17.HD1/HE2	A3.O1P	2.10±0.05	6
R23.HH*	C4.O2P	2.20±0.20	5
T46.O	C4.H4*	2.45±0.20	5
A55.O	U2.HN3	2.20±0.05	6
F57.HN	U2.O4	2.00±0.05	7
T69.O	C4.H4*	2.25±0.20	9
R73.HH*	U2.O2′	2.05±0.20	9
R73.HH*	A3.O5′	1.95±0.15	9
D75.OD*	U2.HO2′	1.85±0.05	9
K83[b].HZ*	A1.O5′	2.25±0.35	6
B. *Hydrophobic contacts (C–C distance ≤3.9 Å)*			
D12.side[c]	A5.ribose[c]	3.70±0.15	6
Q20.side	A5.ribose	3.70±0.15	5
G21.main[c]	A5.ribose	3.60±0.20	9
T22.side	A5.base[c]	3.70±0.15	5
R23.side	C4.ribose	3.75±0.10	8
T37[b].main/side	U2.ribose	3.65±0.10	5
R38[b].side	A1.ribose	3.75±0.10	5
T46.side	A3.base	3.40±0.30	5
T46.side	C4.ribose	3.70±0.15	5
T46.main/side	C4.base	3.65±0.15	10
S47.main/side	A3.base	3.65±0.15	8
V71.side	A3.base	3.60±0.20	6
R73.side	A3.base	3.60±0.20	7

Contacts are reported if found in at least five out of the ten Kid–RNA models obtained with HADDOCK.[30]

[a] Occurrence of the hydrogen bond or C–C contact in the ensemble of ten models.

[b] K83, T37 and R38 belong to monomer B.

[c] Whether main-chain or side-chain atoms of Kid residues are involved in the hydrophobic contact is denoted main and side. Atoms belonging to the nucleotide ribose or base parts are called accordingly.

and T1[24]). After the final clustering, the lowest energy cluster contained 72 structures. The lowest energy structure of this cluster with no AIR violations larger than 0.1 Å is depicted in Figure 4(c). The overall structure of the Kid–RNA complex is identical with the complex obtained after the first docking run. The ten best structures of the cluster (PDB: 2C06) were analysed and the hydrogen bonds and hydrophobic contacts observed in at least 50% of the structures are reported in Table 2.

Kid–RNA interactions involved in RNA recognition and binding

Four hydrogen bonds and five hydrophobic contacts were detected between Kid and the bases of the central three nucleotides UAC of the RNA fragment (see Table 2). These interactions are likely to be important for selective recognition of 5′-UA(A/C)-3′ sequences. The hydrogen bonds, depicted in Figure 4(d), are located between Kid A55 and F57, and two uracil-specific base atoms, and between the backbone of T46 and T69 and the cytosine base amino protons H41/H42. Adenosine also possesses an NH_2 group at a similar position, explaining the Kid preference for either adenosine or cytosine as third nucleotide of the 5′-UA(A/C)-3′ sequence. Less defined interactions of the side-chain H atoms of R73 with the UA fragment exist as well. The hydrophobic contacts are found between T46 and cytosine 4, and T46/S47/V71/R73 and adenosine 3. Sequence alignments of Kid with MazF and related toxins reveal that Kid T46 is highly conserved.[14,15,31] Since T46 displays specific interactions with adenosine 3 and cytosine 4, it probably plays a key role in recognising NAC sites, the RNA cleavage site of all three RNases Kid, MazF and ChpBK. S47 (moderately conserved) and V71 (highly conserved) display hydrophobic interactions with the adenosine-specific C2 of adenosine 3, conserved in the majority of sequences cleaved by Kid or related toxins. Combining the information provided by hydrogen bonds and hydrophobic interactions, A55/R73 (not conserved), S47/F57 (moderately conserved) and V71 are likely to promote selectivity towards uracil at position 2 and adenosine at position 3.

Seven hydrogen bonds between Kid and the RNA backbone (see Table 2) are also important for positioning of the RNA in the binding pocket of Kid. Those are located between K83 (of monomer B) and adenosine 1, R73/D75 and uracil 2, H17/R73 and adenosine 3, R23 and cytosine 4, and D12 and adenosine 5. Hydrophobic contacts are observed between D12/Q20/G21 and the ribose of adenosine 5, R23/T46 and the ribose of cytosine 4, and T37/R38 (of monomer B) and the ribose moieties of uracil 2 and adenosine 1, respectively (see Table 2). Interestingly, G21 is highly conserved and a G21R mutation inactivates the Kid enzyme.[14,29] The large arginine side-chain most likely occupies the space needed for a nucleotide at this position.

Kid–RNA interactions responsible for RNA cleavage

A representation of the active site of Kid, based on the HADDOCK result depicted in Figure 4(d) and (e), is shown in Figure 5(a). Figure 5(b) and (c) show the active sites of RNase A and RNase T1, respectively, both similar to that of Kid, despite a lack of obvious overall structural similarity between the three proteins.[24] Among the most prominent hydrogen bonds in Table 2 are those located between the side-chain of R73 and the 5′-O of adenosine 3, and the side-chain of D75 and the 2′-OH of uracil 2. D75, being the only surface-accessible, negatively charged residue within the predominantly positively charged RNA-binding pocket of Kid, obviously acts as the catalytic base of the Kid toxin, while R73 acts as the catalytic acid. Possessing two NH_2 groups, R73 fulfils a second function in the Kid cleavage mechanism: like K41 in RNase A and H40 in RNase T1, it reduces the pK_a of the 2′-OH group by donating a charged hydrogen bond to the 2′-O, thereby facilitating proton transfer from the uracil 2′-OH group to the general base.[24] The side-chain of H17 is located within the active site of Kid as well. It is doubly protonated (measured by ^{1}H–^{15}N ^{3}J-NMR[32] in the absence of RNA, data not shown) and forms a hydrogen

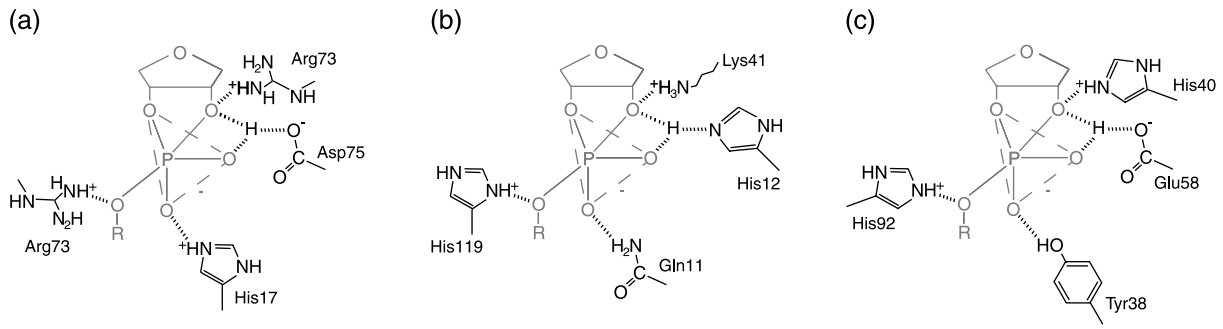

Figure 5. A representation of the active site of (a) Kid, (b) RNase A and (c) RNase T1 with RNA atoms in grey and Kid atoms in black. Shown is the pentavalent transition state: the 3′-O and two non bridging oxygen atoms form a trigonal bipyramid (broken grey lines), while the attacking 2′-O and leaving 5′-O take up apical positions.[24] Catalytic hydrogen bonds are depicted as broken black lines. See the text for details.

bond to the O1P of adenosine 3. It is therefore functionally similar to Q11 in RNase A and to Y38 in RNase T1.[24] H17 was not observed to be essential for Kid toxicity in the previously reported mutagenesis study,[14,29] but the method used allows only histidine to tyrosine mutations. A H17Y mutant would retain hydrogen-bonding capacity and would therefore not affect Kid cleavage activity significantly. Q19 and Q76 are also located near the cleavage site, but their specific role is not clear, since they are not involved in well-defined hydrogen bonds. Although E18, D81 and R85 are essential for Kid toxicity, they do not play a role in the Kid active site. It has been reported that disruption of the salt-bridge between E18 of monomer A and R85 of monomer B would cause a substantial destabilisation of the dimer interface.[14,29] Since this interface is part of the concatenated RNA-binding pocket needed for Kid activity, neither E18 nor R85 is able to participate in Kid cleavage. Residue D81 of monomer B points away from the RNA-binding pocket and forms a hydrogen bond with the backbone of H17 of monomer A. It is therefore likely to be involved in dimer stabilisation as well.

Sequence alignments show that D75 of Kid is conserved in MazF (D76).[14,15,31] Also most other related toxins possess an acidic residue (D or E) at this position that can act as the catalytic base. ChpBK, however, lacks this acidic residue and contains glutamine instead. This fits with the fact that ChpBK has reduced endoribonuclease activity compared to MazF.[22] The catalytic acid of Kid, R73, is not conserved among the Kid homologues. Speculation about the basic residues involved in catalysis by MazF, ChpBK and other related toxins would require more knowledge about the structures of these proteins in their active conformation. Q19 and Q76 are both conserved in most related proteins, while a histidine residue or a functionally similar serine residue is found at the position corresponding to H17 of Kid.

Although a high level of structural resemblance exists between Kid, MazF and CcdB,[14,15,33] the function of the CcdB toxin is rather different. Instead of cleaving RNA, CcdB is involved in gyrase poisoning.[34–37] The fact that CcdB lacks numerous amino acids responsible for RNase activity points out that it cannot be an RNase like Kid or MazF. Finally, we would like to remark that Kid might be able to act on the codon sitting at the ribosomal A-site like the toxin RelE,[38] since it can target just a minimal substrate as UpA. However, a recent study on the aRelE–aRelB TA complex shows that aRelE has dimensions and shape comparable with those of the decoding domain in EF-G, suggesting that they enter the ribosomal A-site in a similar way (Takai *et al.*, 2005). The different structure and geometry of the RNA-binding pocket of Kid, described in this work, could make this toxin less efficient in targeting RNA located in the A-site of the ribosome. This is underlined by the different way in which the aRelB and Kis antitoxins neutralise the aRelE and Kid toxins: while aRelB inhibits the RNase activity of aRelE by extensively wrapping around the toxin such that it becomes too large to enter into the ribosomal A-site.[39] Kis inhibits RNA cleavage by Kid in a more direct way, by partly occupying one RNA-binding site while imposing the disruption of the second binding pocket of the Kid dimer. Furthermore, Kid is active as a dimer with a size comparable to that of the aRelE–aRelB heterodimer. Therefore it seems very likely that Kid and its homologue MazF are more effective in ribosome-independent RNA cleavage.

Concluding remarks

We have shown that the Kid toxin cleaves RNA yielding two fragments; one with a 2′:3′-cyclic phosphate group and one with a free 5′-OH group. The cleavage mechanism is similar to the mechanism of RNases A and T1, involving the uracil 2′-OH group. We have demonstrated that residues of both monomers of the Kid dimer together form a concatenated RNA-binding surface and provided a detailed picture of the position of the AUACA fragment within this binding pocket. We propose that residues D75, R73 and H17 form the active site of the Kid toxin. With the help of R73, the catalytic base D75 deprotonates the 2′-OH group of uracil, which subsequently performs a nucleophilic attack on the electrophilic phosphorus.

The transphosphorylation reaction is complete after donation of a hydrogen atom by the catalytic acid R73 to the adenosine 5′-O. H17 stabilises the complex, and residues T46, S47, A55, F57, T69, V71 and R73 preserve the RNA sequence-specificity.

Materials and Methods

Sample preparation

^{15}N-labelled Kid toxin and Kis antitoxin were expressed by growing phototrophic *E. coli* TG1 cells carrying the pRG-recA-NHis plasmid[40] in M9 minimal medium containing $^{15}NH_4Cl$ (98+% pure, Cambridge Isotope Laboratories), for 24 h at 37 °C. The isotope-labelled proteins were purified essentially as described for unlabelled Kid and Kis.[13] The hexahistidine-tagged Kis was eluted from the Ni-affinity column using 20 mM Tris–HCl (pH 8.0), 50 mM EDTA, 5 M guanidine-HCl, and. Kis was refolded as described for Kid and subsequently the histidine-tag was cleaved off by thrombin. Further purification of the Kis protein was accomplished as described for Kid, using a Q-Sepharose column (Pharmacia) instead of an SP-Sepharose column. The proteins were subsequently dialysed against NMR buffer (100 mM deuterated sodium acetate buffer, pH 5.8). NaCD3COOD (99.96% pure) and ^2H_2O (99.9% pure) were obtained from Cambridge Isotope Laboratories and NaC^{2}H 3COO (99+% pure) was obtained from Aldrich. The mononucleotide 5′-AMP, dinucleotide UpA and a mixture of 39% 2′:3′-cUMP, 30% 3′-UMP, 20% 2′-UMP and 10%U were obtained from Sigma. Both 5′-AMP and 2′:3′-cUMP were in the free acid form, and UpA was used as tributylammonium salt. The nucleotides were dissolved in NMR buffer in concentrations varying between 11 mM and 20 mM, determined spectrophotometrically. The single-stranded 5 nt RNA (AUACA), RNA-dU (AdUACA) and DNA (d(AUACA)) oligonucleotides were obtained from Eurogentec S.A. and stock-solutions of 10 mM were prepared in NMR buffer.

NMR experiments

All spectra were recorded on a Bruker Avance 750 spectrometer equipped with a TXI probe with *xyz*-gradients, at 30 °C. The 1D spectra were processed and analysed with the program XWINNMR3.5 (Bruker). All 2D spectra were processed with the NMRPIPE software package[41] and analysed with NMRView.[42]

Assignments of the Kid chemical shifts

NMR assignments of $^{13}C/^{15}N$-labelled Kid in 100 mM KPi buffer (pH 5.8) were obtained and analysed with the program TALOS,[43] enabling the prediction of the secondary structure of the Kid protein in solution, as will be described elsewhere (M.B.K. *et al*., unpublished results). The $^1H–^{15}N$ chemical shifts of Kid are added as Supplementary Data.

^{1}H measurements to study the RNA cleavage ability of Kid

Series of 1D ^{1}H-NMR spectra were recorded of samples containing 7.7 μM Kid and one of the 5 nt RNAs (AUACA), RNA-dU (AdUACA) or DNA (d(AUACA)) fragments at 90 μM in NMR buffer with 5% ^2H_2O. For each series, the time elapsed between the addition of the Kid protein to the oligonucleotide sample and the first pulse of the first 1D experiment was measured precisely. Each 1D spectrum contained 16,384 points with a spectral width of 12019 Hz and lasted 2 min to record. The duration of the whole series was 3 h in the case of RNA and DNA and 30 h in case of RNA-dU.

For the experiment with the RNA oligonucleotide, polynomial functions were fit (Kaleidagraph, Synergy Software) to the peak intensities of the HC protons of the bases of substrate and products plotted against time. Eadie–Hofstee plots revealed the K_m and V_{max} values for the cleavage reactions performed by the Kid toxin. The DNA cleavage experiment showed no differences between the first and last spectrum recorded, and was omitted for further analyses. The RNA cleavage experiment was repeated in the presence of 7.2 μM antitoxin Kis. This series lasted 22 h and was analysed as described above.

The products of the UpA cleavage reaction by Kid were identified by comparing the 1D ^{1}H-NMR spectrum of cleaved UpA with the spectra of the mononucleotides 5′-AMP and a 2′:3′-cUMP mixture. The assignment of the compounds of the 2′:3′-cUMP mixture was made by comparing the integrals in the ^{1}H-NMR spectrum with the ratios stated by Sigma.

$^1H–^{15}N$ HSQC measurements to map Kid–ligand interactions

For the chemical shift perturbation experiments, ^{15}N-labelled Kid samples containing approximately 200 μM protein in NMR buffer with 5% ^2H_2O were used. The 2D $^{15}N–^1H$ HSQC spectra were recorded on ^{15}N-labelled Kid alone and with different amounts of ligand added to the sample, such that the Kid to ligand ratios varied from 1:0 to 1:2 for the RNA-dU and 1:4 for the DNA oligonucleotides. For all $^{15}N–^1H$-HSQC spectra, 1024 points with a spectral width of 4281 Hz in the direct dimension and 200 points with a spectral width of 2509 Hz in the indirect dimension were recorded. The number of scans was eight for the measurements of the RNA-dU and 16 for DNA titrations. Chemical shift perturbations in the ^{1}H and ^{15}N dimensions were combined to a weighted composite shift change:[44]

$$\Delta = \sqrt{((\delta H)^2 + (\delta N/6.51)^2)}$$

Docking

Docking of the RNA AUACA oligonucleotide into the RNA-binding pocket of Kid was performed using a development version of the software HADDOCK (Haddock2.0_devel),[30,45] in combination with CNS[46] based on chemical shift perturbation data observed for Kid upon addition of RNA-dU, knowledge about the Kid cleavage reaction and previously identified non-toxic Kid mutants.[29] The starting structures for the docking were ten models of Kid generated from the Kid crystal structure (PDB code 1M1F)[14] using the program Modeller6v2[47] and a model of the RNA AUACA fragment constructed with the Nucleic Acid Builder package (v 4.6).[48] Active and passive Kid residues for the definition of interaction restraints were chosen based on the chemical shift perturbation data and solvent accessi-

bility (Table 1). Residues of which the amide atoms displayed intermediate exchange behaviour were selected as active residues if their solvent accessibility was higher than 12% for at least one of the monomers, as calculated using the program NACCESS (Hubbard & Thornton, 1993). Amino acids of the loop comprising residues S47 to A55 were defined as passive together with residue A58 located beneath this loop and not identified to be essential for Kid toxicity in the previously reported mutagenesis study.[14,29] All solvent-accessible (>12%) neighbouring amino acid residues were selected as passive residues. A 2 Å distance was used to define the ambiguous interaction restraints (AIRs). For the RNA fragment, the three central nucleotides UAC were selected as active residues, since cleavage takes places only at 5′-UA(A/C)-3′ sequences. AIRs were defined solely from the unique base atoms of the uracil and adenosine to suitable Kid atoms (i.e. from H to N or O and *vice versa*), while for cytosine the whole base was selected because of the lower specificity of this nucleotide in the sequences that are cleaved by Kid. The two flanking adenosine nucleotides were selected as passive residues. Additional AIRs of 1.7 Å distance were defined based on knowledge about the Kid cleavage mechanism in combination with the mutational analysis, requiring that the uracil 2′-OH group must be close to either E18, D75 or D81 and the 5′-O of adenosine must be close to R73 or R85. Residues 47–55 of both Kid monomers and the complete RNA fragment were defined as fully flexible segments. During the rigid body energy minimisation, 1000 structures were calculated and the 200 best solutions based on the intermolecular energy were used for the semi-flexible, simulated annealing followed by an explicit water refinement. The solutions were clustered in two steps using a 3.5 Å RMSD based on the pairwise backbone RMSD matrix calculated first for the fourth nucleotide and subsequently for nucleotides 2 and 3 of the RNA fragment after superposition on the backbone of Kid. Based on visual inspection, 30 out of the 34 structures of the lowest energy cluster were used as input for a second semi-flexible, simulated annealing run followed by an explicit water refinement. Three extra restraints, based on the Kid cleavage mechanism, were added to obtain a proper geometry of the RNA within the active site of Kid. A 2 Å distance was used for AIRs between the uracil 2′-O and any HN- or HO-atom of Kid, between the adenosine O1P and any HN- or HO-atom of Kid, and between the uracil 2′-OH and adenosine O2P. The final 120 solutions were clustered as described before.

Analysis of the intermolecular contacts

Intermolecular contacts between Kid residues and RNA nucleotides were analysed using standard HADDOCK analysis scripts.[30] A 3.9 Å heavy-atoms distance cut-off was used for hydrophobic contacts and a 2.7 Å proton–acceptor distance cut-off for hydrogen bonds.

Analysis of cleavage products by electrospray ionisation mass spectrometry

The products of the RNA and RNA-dU cleavage reactions by Kid were identified using electrospray ionisation mass spectrometry essentially as described.[49–51] Nanoflow electrospray needles were made from borosilicate glass capillaries (Kwik-Fil, World Precision Instruments) on a P-97 puller (Sutter Instruments, USA). Needles were coated with a thin layer of gold (500 Å) by using a Scancoat Six sputter coater (Edwards High Vacuum International). Samples were prepared in 250 mM ammonium acetate (pH 6.8) and incubated at 21 °C. Kid and RNA or RNA-dU were mixed to a final concentration of 20 μM or 50 μM, respectively. Aliquots of the mixture were collected at different times and introduced into a nanoflow electrospray ionisation orthogonal time-of-flight mass spectrometer (Micromass LC-T, Waters) without further treatment. The products were analysed in positive ion mode. Nanoflow electrospray voltages were optimised for transmission of RNA (capillary voltage 1200 V and cone voltage 30–50 V). The experiment was repeated in presence of the antitoxin Kis (6.25 μM and 12.5 μM). To monitor formation of the Kid–RNA complex, 2.5 μM Kid and 5 μM or 25 μM RNA were incubated at 21 °C for 2 min and the mixture was introduced into the LC-T mass spectrometer without further treatment. With the aim to produce intact ions *in vacuo* from protein complexes in solution, the ions were cooled by increasing the pressure in the first vacuum stages of the mass spectrometer (Tahallah, 2001) (source pressure 8 mbar: 1 bar = 10^5 Pa). Nanoflow electrospray voltages were optimised for transmission of RNA (capillary voltage 1400 V and cone voltage 150–200 V).

Data Bank accession code

The chemical shifts of Kid at pH 5.8 and 303 K have been deposited in the BioMag Res Bank under accession number BMRB-6925. The coordinates of the ten best structural models of the Kid–RNA complex have been deposited in the EBI Macromolecular Structure Database (accession code 2C06) together with the AIR restraints.

Acknowledgements

We thank A. D. van Dijk and M. van Dijk for their help regarding the docking calculations, and G. E. Folkers and V. L. Hsu for valuable discussions. This project was supported financially by the European Union (QLK2-CT-2000-00634, HPRI-CT-2001-00172 and NMR Large Scale Facility scheme), the Netherlands Organisation for Scientific Research NWO/CW and the Center for Biomedical Genetics. Additional support to the laboratory of R.D.-O. was provided by the Spanish MCyT (SAF2002-04649) and MEC (BFU2005-03911/BMC). M.C.M. was supported by a EU Marie Curie Fellowship (HPMT-CT-2001-00389) and R.H.H. vd H. by a VENI fellowship (700.54.402) from the Netherlands Organisation for Scientific Research (NWO).

Supplementary Data

Supplementary data associated with this article can be found, in the online version, at doi:10.1016/j.jmb.2005.12.033

References

1. Hayes, F. (2003). Toxins–antitoxins: plasmid maintenance, programmed cell death, and cell cycle arrest. *Science*, **301**, 1496–1499.
2. Gerdes, K., Christensen, S. K. & Lobner-Olesen, A. (2005). Prokaryotic toxin–antitoxin stress response loci. *Nature Rev. Microbiol.* **3**, 371–382.
3. Anantharaman, V. & Aravind, L. (2003). New connections in the prokaryotic toxin–antitoxin network: relationship with the eukaryotic nonsense-mediated RNA decay system. *Genome Biol.* **4**, R81.
4. Engelberg-Kulka, H. & Glaser, G. (1999). Addiction modules and programmed cell death and antideath in bacterial cultures. *Annu. Rev. Microbiol.* **53**, 43–70.
5. Pandey, D. P. & Gerdes, K. (2005). Toxin–antitoxin loci are highly abundant in free-living but lost from host-associated prokaryotes. *Nucl. Acids Res.* **33**, 966–976.
6. de la Cueva-Mendez, G., Mills, A. D., Clay-Farrace, L., Diaz-Orejas, R. & Laskey, R. A. (2003). Regulatable killing of eukaryotic cells by the prokaryotic proteins Kid and Kis. *EMBO J.* **22**, 246–251.
7. Picardeau, M., Le Dantec, C., Richard, G. F. & Saint Girons, I. (2003). The spirochetal chpK-chromosomal toxin–antitoxin locus induces growth inhibition of yeast and mycobacteria. *FEMS Microbiol Letters*, **229**, 277–281.
8. Yamamoto, T. A., Gerdes, K. & Tunnacliffe, A. (2002). Bacterial toxin RelE induces apoptosis in human cells. *FEBS Letters*, **519**, 191–194.
9. Bravo, A., de Torrontegui, G. & Diaz, R. (1987). Identification of components of a new stability system of plasmid R1, ParD, that is close to the origin of replication of this plasmid. *Mol. Gen. Genet.* **210**, 101–110.
10. Tsuchimoto, S., Ohtsubo, H. & Ohtsubo, E. (1988). Two genes, pemK and pemI, responsible for stable maintenance of resistance plasmid R100. *J. Bacteriol.* **170**, 1461–1466.
11. Bravo, A., Ortega, S., de Torrontegui, G. & Diaz, R. (1988). Killing of *Escherichia coli* cells modulated by components of the stability system ParD of plasmid R1. *Mol. Gen. Genet.* **215**, 146–151.
12. Ruiz-Echevarria, M. J., Berzal-Herranz, A., Gerdes, K. & Diaz-Orejas, R. (1991). The kis and kid genes of the parD maintenance system of plasmid R1 form an operon that is autoregulated at the level of transcription by the co-ordinated action of the Kis and Kid proteins. *Mol. Microbiol.* **5**, 2685–2693.
13. Hargreaves, D., Giraldo, R., Santos-Sierra, S., Boelens, R., Rice, D. W., Diaz Orejas, R. & Rafferty, J. B. (2002). Crystallization and preliminary X-ray crystallographic studies on the parD-encoded protein Kid from *Escherichia coli* plasmid R1. *Acta Crystallog. sect. D*, **58**, 355–3558.
14. Hargreaves, D., Santos-Sierra, S., Giraldo, R., Sabariegos-Jareno, R., de la Cueva-Mendez, G., Boelens, R. *et al*. (2002). Structural and functional analysis of the kid toxin protein from *E. coli* plasmid R1. *Structure (Camb.)*, **10**, 1425–1433.
15. Kamada, K., Hanaoka, F. & Burley, S. K. (2003). Crystal structure of the MazE/MazF complex: molecular bases of antidote–toxin recognition. *Mol. Cell*, **11**, 875–884.
16. Christensen, S. K., Pedersen, K., Hansen, F. G. & Gerdes, K. (2003). Toxin–antitoxin loci as stress-response-elements: ChpAK/MazF and ChpBK cleave translated RNAs and are counteracted by tmRNA. *J. Mol. Biol.* **332**, 809–819.
17. Munoz-Gomez, A. J., Lemonnier, M., Santos-Sierra, S., Berzal-Herranz, A. & Diaz-Orejas, R. (2005). RNase/anti-RNase activities of the bacterial parD toxin–antitoxin system. *J. Bacteriol.* **187**, 3151–3157.
18. Munoz-Gomez, A. J., Santos-Sierra, S., Berzal-Herranz, A., Lemonnier, M. & Diaz-Orejas, R. (2004). Insights into the specificity of RNA cleavage by the *Escherichia coli* MazF toxin. *FEBS Letters*, **567**, 316–320.
19. Pimentel, B., Madine, M. A. & de la Cueva-Mendez, G. (2005). Kid cleaves specific mRNAs at UUACU sites to rescue the copy number of plasmid R1. *EMBO J.* **24**, 3459–3469.
20. Zhang, J., Zhang, Y., Zhu, L., Suzuki, M. & Inouye, M. (2004). Interference of mRNA function by sequence-specific endoribonuclease PemK. *J. Biol. Chem.* **279**, 20678–20684.
21. Zhang, Y., Zhang, J., Hara, H., Kato, I. & Inouye, M. (2005). Insights into the mRNA cleavage mechanism by MazF, an mRNA interferase. *J. Biol. Chem.* **280**, 3143–31450.
22. Zhang, Y., Zhu, L., Zhang, J. & Inouye, M. (2005). Characterization of ChpBK, an mRNA interferase from *Escherichia coli*. *J. Biol. Chem.* **280**, 26080–26088.
23. Zhang, Y., Zhang, J., Hoeflich, K. P., Ikura, M., Qing, G. & Inouye, M. (2003). MazF cleaves cellular mRNAs specifically at ACA to block protein synthesis in *Escherichia coli*. *Mol. Cell*, **12**, 913–923.
24. Loverix, S. & Steyaert, J. (2003). Ribonucleases: from prototypes to therapeutic targets? *Curr. Med. Chem.* **10**, 779–785.
25. Steyaert, J. (1997). A decade of protein engineering on ribonuclease T1-atomic dissection of the enzyme–substrate interactions. *Eur. J. Biochem.* **247**, 1–11.
26. Raines, R. T. & Ribonuclease, A. (1998). *Chem. Rev.* **98**, 1045–1066.
27. Loverix, S. & Steyaert, J. (2001). Deciphering the mechanism of RNase T1. *Methods Enzymol.* **341**, 305–323.
28. Vicentini, A. M., Hemmings, B. A. & Hofsteenge, J. (1994). Residues 36-42 of liver RNase PL3 contribute to its uridine-preferring substrate specificity. Cloning of the cDNA and site-directed mutagenesis studies. *Protein Sci.* **3**, 459–466.
29. Santos-Sierra, S., Lemonnier, M., Nunez, B., Hargreaves, D., Rafferty, J., Giraldo, R. *et al*. (2003). Non-cytotoxic variants of the Kid protein that retain their auto-regulatory activity. *Plasmid*, **50**, 120–130.
30. Dominguez, C., Boelens, R. & Bonvin, A. M. (2003). HADDOCK: a protein–protein docking approach based on biochemical or biophysical information. *J. Am. Chem. Soc.* **125**, 1731–1737.
31. Gerdes, K. (2000). Toxin–antitoxin modules may regulate synthesis of macromolecules during nutritional stress. *J. Bacteriol.* **182**, 561–572.
32. Pelton, J. G., Torchia, D. A., Meadow, N. D. & Roseman, S. (1993). Tautomeric states of the active-site histidines of phosphorylated and unphosphorylated IIIGlc, a signal-transducing protein from *Escherichia coli*, using two-dimensional heteronuclear NMR techniques. *Protein Sci.* **2**, 543–558.
33. Loris, R., Dao-Thi, M. H., Bahassi, E. M., Van Melderen, L., Poortmans, F., Liddington, R. *et al*. (1999). Crystal structure of CcdB, a topoisomerase poison from *E. coli*. *J. Mol. Biol.* **285**, 1667–1677.
34. Dao-Thi, M. H., Van Melderen, L., De Genst, E., Afif, H., Buts, L., Wyns, L. & Loris, R. (2005). Molecular basis of gyrase poisoning by the addiction toxin CcdB. *J. Mol. Biol.* **348**, 1091–1102.

35. Van Melderen, L. (2002). Molecular interactions of the CcdB poison with its bacterial target, the DNA gyrase. *Int. J. Med. Microbiol.* **291**, 537–544.
36. Bahassi, E. M., O'Dea, M. H., Allali, N., Messens, J., Gellert, M. & Couturier, M. (1999). Interactions of CcdB with DNA gyrase. Inactivation of Gyra, poisoning of the gyrase–DNA complex, and the antidote action of CcdA. *J. Biol. Chem.* **274**, 10936–10944.
37. Bernard, P., Kezdy, K. E., Van Melderen, L., Steyaert, J., Wyns, L., Pato, M. L. *et al*. (1993). The F plasmid CcdB protein induces efficient ATP-dependent DNA cleavage by gyrase. *J. Mol. Biol.* **234**, 534–541.
38. Pedersen, K., Zavialov, A. V., Pavlov, M. Y., Elf, J., Gerdes, K. & Ehrenberg, M. (2003). The bacterial toxin RelE displays codon-specific cleavage of mRNAs in the ribosomal A site. *Cell*, **112**, 131–140.
39. Takagi, H., Kakuta, Y., Okada, T., Yao, M., Tanaka, I. & Kimura, M. (2005). Crystal structure of archaeal toxin–antitoxin RelE–RelB complex with implications for toxin activity and antitoxin effects. *Nature Struct. Mol. Biol.* **12**, 327–331.
40. Giraldo, R., Andreu, J. M. & Diaz-Orejas, R. (1998). Protein domains and conformational changes in the activation of RepA, a DNA replication initiator. *EMBO J.* **17**, 4511–4526.
41. Delaglio, F., Grzesiek, S., Vuister, G. W., Zhu, G., Pfeifer, J. & Bax, A. (1995). NMRPipe: a multi-dimensional spectral processing system based on UNIX pipes. *J. Biomol. NMR*, **6**, 277–293.
42. Johnson, B. A. & Blevins, R. A. (1994). NMRView: a computer program for the visualization and analysis of NMR data. *J. Biomol. NMR*, **4**, 603–614.
43. Cornilescu, G., Delaglio, F. & Bax, A. (1999). Protein backbone angle restraints from searching a database for chemical shift and sequence homology. *J. Biomol. NMR*, **13**, 289–302.
44. Mulder, F. A., van Tilborg, P. J., Kaptein, R. & Boelens, R. (1999). Microsecond time scale dynamics in the RXR DNA-binding domain from a combination of spin-echo and off-resonance rotating frame relaxation measurements. *J. Biomol. NMR*, **13**, 275–288.
45. van Dijk, A. D., Boelens, R. & Bonvin, A. M. (2005). Data-driven docking for the study of biomolecular complexes. *FEBS J.* **272**, 293–312.
46. Brunger, A. T., Adams, P. D., Clore, G. M., DeLano, W. L., Gros, P., Grosse-Kunstleve, R. W. *et al*. (1998). Crystallography & NMR system: a new software suite for macromolecular structure determination. *Acta Crystallog. sect. D*, **54**, 905–921.
47. Fiser, A., Do, R. K. & Sali, A. (2000). Modeling of loops in protein structures. *Protein Sci.* **9**, 1753–1773.
48. Macke, T. & Case, D. A. (1998). Modeling unusual nucleic acid structures. In *Molecular Modeling of Nucleic Acid* (Leontes, N. B. & SantaLucia, J., Jr, eds), pp. 379–393, American Chemical Society, Washington, DC.
49. Ni, J., Pomerantz, C., Rozenski, J., Zhang, Y. & McCloskey, J. A. (1996). Interpretation of oligonucleotide mass spectra for determination of sequence using electrospray ionization and tandem mass spectrometry. *Anal. Chem.* **68**, 1989–1999.
50. McCloskey, J. A., Whitehill, A. B., Rozenski, J., Qiu, F. & Crain, P. F. (1999). New techniques for the rapid characterization of oligonucleotides by mass spectrometry. *Nucleos. Nucleot.* **18**, 1549–1553.
51. van den Heuvel, R. H., Gato, S., Versluis, C., Gerbaux, P., Kleanthous, C. & Heck, A. J. (2005). Real-time monitoring of enzymatic DNA hydrolysis by electrospray ionization mass spectrometry. *Nucl. Acids Res.* **33**, e96.
52. Kraulis, P. J. (1991). MOLSCRIPT: a program to produce both detailed and schematic plots of protein structures. *J. Appl. Crystallog.* **24**, 946–950.
53. Merritt, E. A. & Murphy, M. E. (1994). Raster3D version 2.0. A program for photorealistic molecular graphics. *Acta Crystallog. sect. D*, **50**, 869–873.

Edited by D. E. Draper

(Received 2 September 2005; received in revised form 1 December 2005; accepted 8 December 2005)
Available online 27 December 2005